

## Supporting Information

### **Hierarchically Porous MOF-polymer Composites via Interfacial Nanoassembly and Emulsion Polymerization**

*Peng Jin, Wenlong Tan, Jia Huo\*, Tingting Liu, Yu Liang, Shuangyin Wang,\*and Darren Bradshaw\**

#### **S1. Experimental Section**

#### **S2. Preparation and characterization of interfacial nanoassembly/ emulsion polymerization**

#### **S3. Generality of interfacial nanoassembly/ emulsion polymerization**

#### **S4. Knoevenagel condensation reaction catalyzed by ZIF-8-based catalysts**

## S1. Experimental Section

*Materials:* All chemicals were purchased from Sinopharm Chemical Reagent Co. Ltd, China and used without pretreatment unless otherwise mentioned. ZIF-8, UiO-66, Cr-MIL-101, and HKUST-1 were synthesized according to previous reports<sup>1, 2</sup> or with minor modification. Fe<sub>3</sub>O<sub>4</sub> nanoparticles with an average diameter of 10 nm were obtained commercially and used without modification.

*Synthesis of ZIF-8/PS:* Typically, 0.70 g ZIF-8 was dispersed in 6 g deionized (DI) water using ultrasound for 30 min. 0.0761 g of 2,2'-azobisisoheptonitrile (ABVN) was dissolved in a mixture of 3.3 g divinylbenzene (DVB), 2.2 g styrene, and 0.36 g oleic acid, which was subsequently mixed with the ZIF-8 dispersion in a 20 ml sample vial. A stable Pickering emulsion was generated by agitation using a homogenizer at 14500 rpm for 2.5 min. The emulsion was then subsequently polymerized at 65 °C for 20 min. The obtained monolith was repeatedly washed with ethanol and dried at 120 °C under vacuum. For the magnetic ZIF-8/PS, 0.07g of Fe<sub>3</sub>O<sub>4</sub> and 0.63 g ZIF-8 were suspended into DI water using ultrasound prior to addition of the monomer solution as for ZIF-8/PS.

*Synthesis of UiO-66/PS:* Typically, 0.50 g UiO-66 was dispersed in 4 g of DI water by ultrasound for 30 min. 0.0761 g of ABVN was dissolved in a solution of 3.3 g DVB and 2.2 g styrene, and then the two solutions were subsequently mixed in a 20 ml sample vial. A stable Pickering emulsion was generated by agitation using the homogenizer at 14500 rpm for 2.5 min. The resultant emulsion was subsequently polymerized at 65 °C for 20 min. The obtained monolith was repeatedly washed with ethanol and subsequently dried at 120 °C under vacuum.

*Synthesis of Cr-MIL-101/PS:* Typically, 0.0817 g of ABVN was dissolved in the solution of 4.595 g DVB and 0.988 g 4-vinylpyridine. 0.50 g Cr-MIL-101 was dispersed in 4 g DI water by ultrasound for 6 h after which time 0.2 g NaCl was added into it, and then the two solutions were mixed with strong stirring (1000 rpm) in a 20 ml sample vial. A stable Pickering emulsion was generated by agitation using the homogenizer at 14500 rpm for 2.5 min. The resultant emulsion was subsequently polymerized at 65 °C for 20 min. The obtained monolith was repeatedly washed with ethanol and subsequently dried at 120 °C under vacuum.

*Synthesis of HKUST-1/PAM:* 0.30 g HKUST-1 was dispersed in 6 mL xylene by ultrasound for 6 h. Acrylamide (AM, 1.533 g), N,N'-methylenebisacrylamide (MBAM, 0.311 g), and N-isopropylacrylamide (NIPAM, 0.40 g) were dissolved in 4 g of distilled water to obtain the monomer aqueous solution. The HKUST-1 dispersion was added slowly into the monomer aqueous solution followed by addition of 0.2 g of 4,4'-azobis(4-cyanovaleric acid) (ACVA) during stirring (1000 rpm). Stirring was continued for a further 1 min after addition. A stable

Pickering emulsion was generated with agitation using the homogenizer at 14500 rpm for 2.5 min. The resultant emulsion was transferred to a preheated oven at 60 °C for 20 min. After removal from the oven, the obtained monolith was continually washed with acetone using a Soxhlet extractor for 24 h and then dried under vacuum at 120 °C overnight.

*Characterization:* A stable Pickering emulsion was generated using the homogenizer T10 B S25 (IKA) at 14500 rpm for 2.5 min. The phase identification of the samples was performed on a Powder X-ray diffractometer (XRD, D8 Advance) using Cu K $\alpha$  radiation, where the scanning range of the diffraction angle (2-Theta) is 5-50 °. The scanning rate was 4 ° min<sup>-1</sup> and step width of 0.02 ° with 40 mA operation current and 40 kV voltage. Thermogravimetric analysis (TGA) was performed using a HTG-1 (HENVEN) instrument and the sample was heated from room temperature to 800 °C at a rate of 10 °C min<sup>-1</sup> under an air atmosphere. Scanning electron microscopy (SEM) measurements were made on a Hitachi S-4800 thermal field emission scanning electron microscope at an accelerating voltage of 5, 10, or 15 kV. Samples for SEM measurements were attached to the stub using carbon paste and then sputter-coated with a thin layer of conductive gold to improve electrical conductivity. The nitrogen adsorption-desorption isotherms were measured at 77 K with a JW-BK200C (Beijing JWGB Sci.&Tech. Co., Ltd.) gas adsorption analyser after the sample was first degassed at 120 °C overnight. Specific surface areas were determined by the BET method, mesopore size distribution was obtained based on BJH analysis of the desorption branches of the isotherms, and the total pore volumes were determined using the desorption branch of N<sub>2</sub> isotherm at  $p/p^0 = 0.99$  (single point). Gas chromatographic (GC) analysis was performed using a Lunan Ruihong SP-7820 instrument equipped with a flame ionization detector (FID) and an SE-54 column (length = 30 m, inner diameter = 0.32 mm, and film thickness = 0.50  $\mu$ m). The temperature for GC analysis ramped from 60 to 140 °C at 20 °C min<sup>-1</sup> and was held at 140 °C for 1 min; then was heated from 140 to 142 at 1 °C/min; and then ramped to 280 °C at 20 °C min<sup>-1</sup> and was held them at 280 °C for 2 min. Inlet and detector temperatures were set at 280 °C. n-Dodecane was used as an internal standard to calculate reaction conversion.

*Catalytic assessment:* The Knoevenagel reaction between malononitrile and benzaldehyde using the ZIF-8/PS composite as the catalyst was performed in a round bottom flask with magnetic stirring. Typically, a mixture of 0.158 g ZIF-8/PS with 0.2 mL (1.96 mmol) benzaldehyde and 0.2 mL n-dodecane as an internal standard was placed into a 25 mL flask containing 4 mL of toluene. The solution of 0.25 g (3.78 mmol) malononitrile in 1 mL toluene was subsequently added into the flask, and the resultant mixture was stirred for 12 h at room temperature. The sample was taken at specific time intervals and analyzed by GC. After the

reaction, the catalyst was removed from the reaction mixture, washed with ethanol for three times, and dried under vacuum at 120 °C for 8 h prior to being reused.

## S2. Preparation and characterization of ZIF-8/PS via Interfacial Nanoassembly/ Emulsion Polymerization

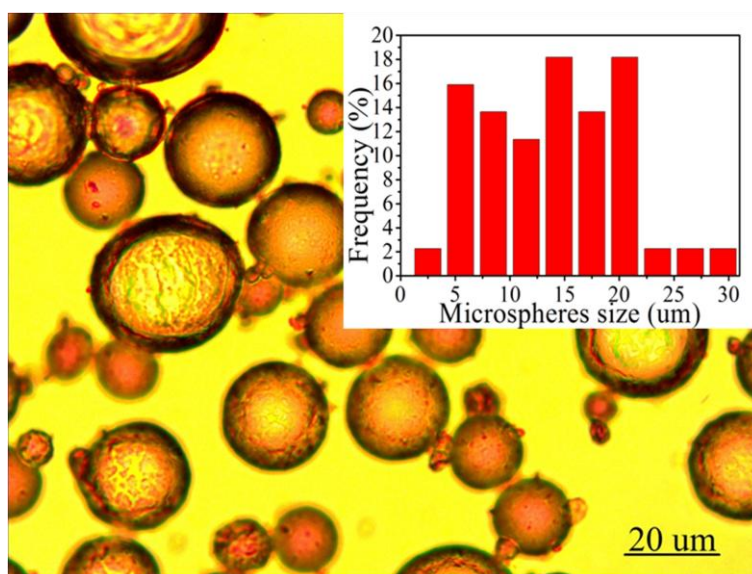


**Figure S1.** Optical microscope image of ZIF-8-stabilized emulsions employed for the preparation of ZIF-8/PS composites through polymerization of the continuous phase. The inset shows the size distribution of the emulsion droplets which ultimately form the macropores within the composites.

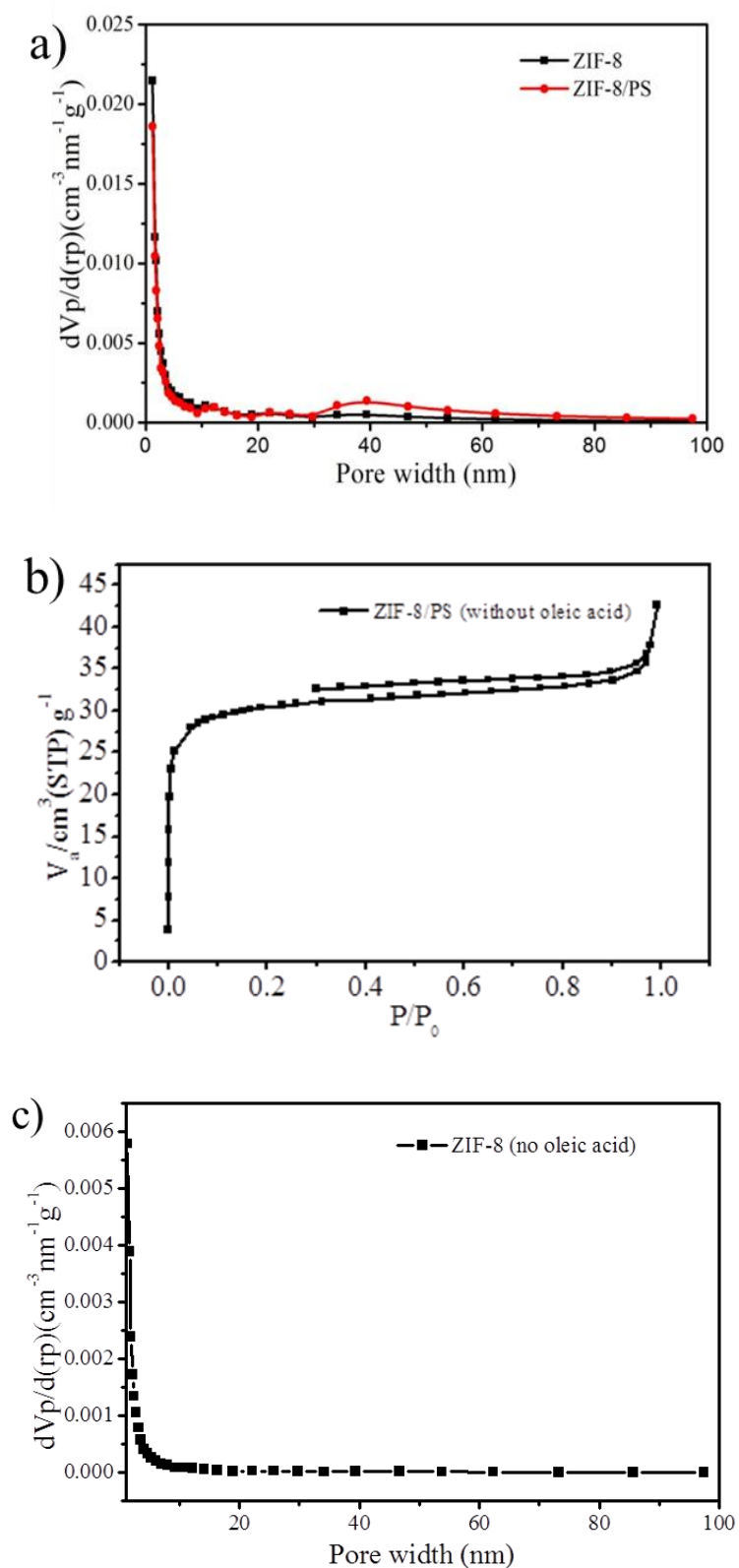


**Figure S2.** (a) BJH mesopore size distribution of ZIF-8 nanoparticles and hierarchically porous ZIF-8/PS composites prepared with oleic acid; (b)  $N_2$  isotherm (Specific surface area is  $118 \text{ m}^2/\text{g}$ ) and (c) mesopore size distribution of ZIF-8/PS prepared without oleic acid demonstrating a reduction in surface area and an absence of mesopores.

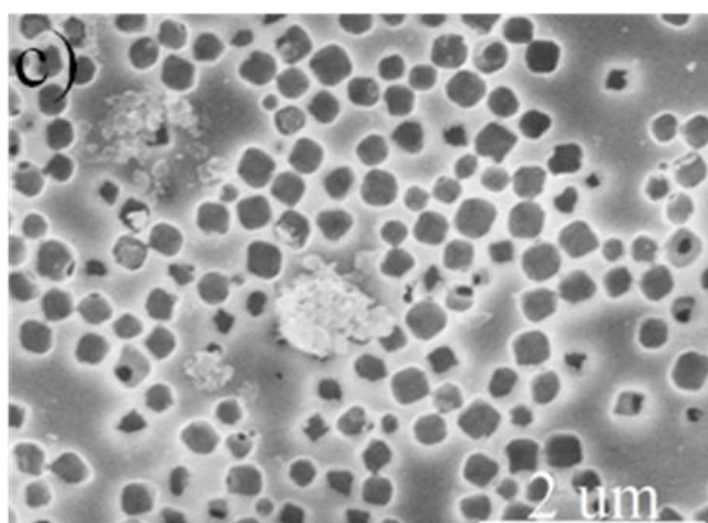
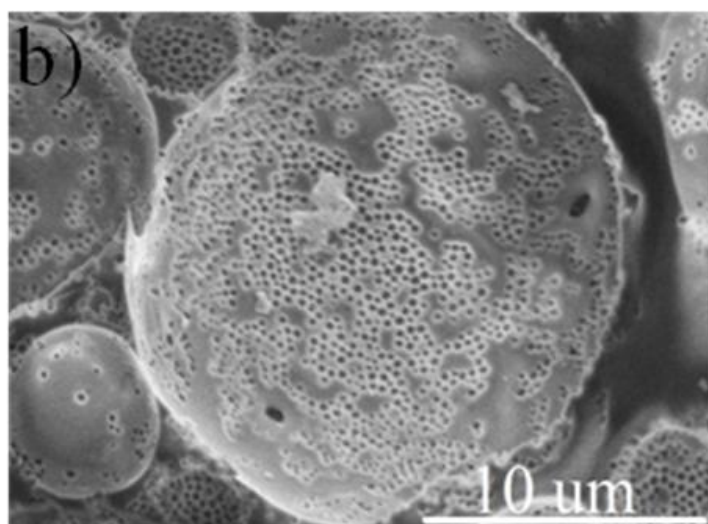
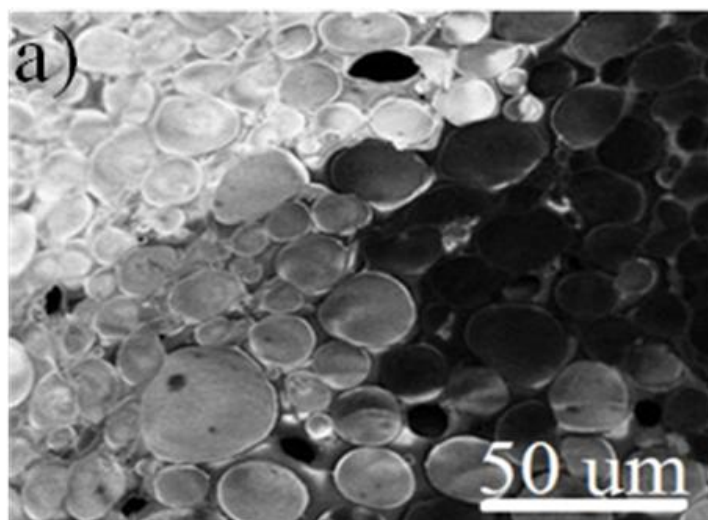


**Figure S3.** Low and high magnification SEM images of the cross-section of hierarchically porous ZIF-8/PS after removal of the ZIF-8 particles by acetic acid dissolution, further confirming their localisation within the macropores.

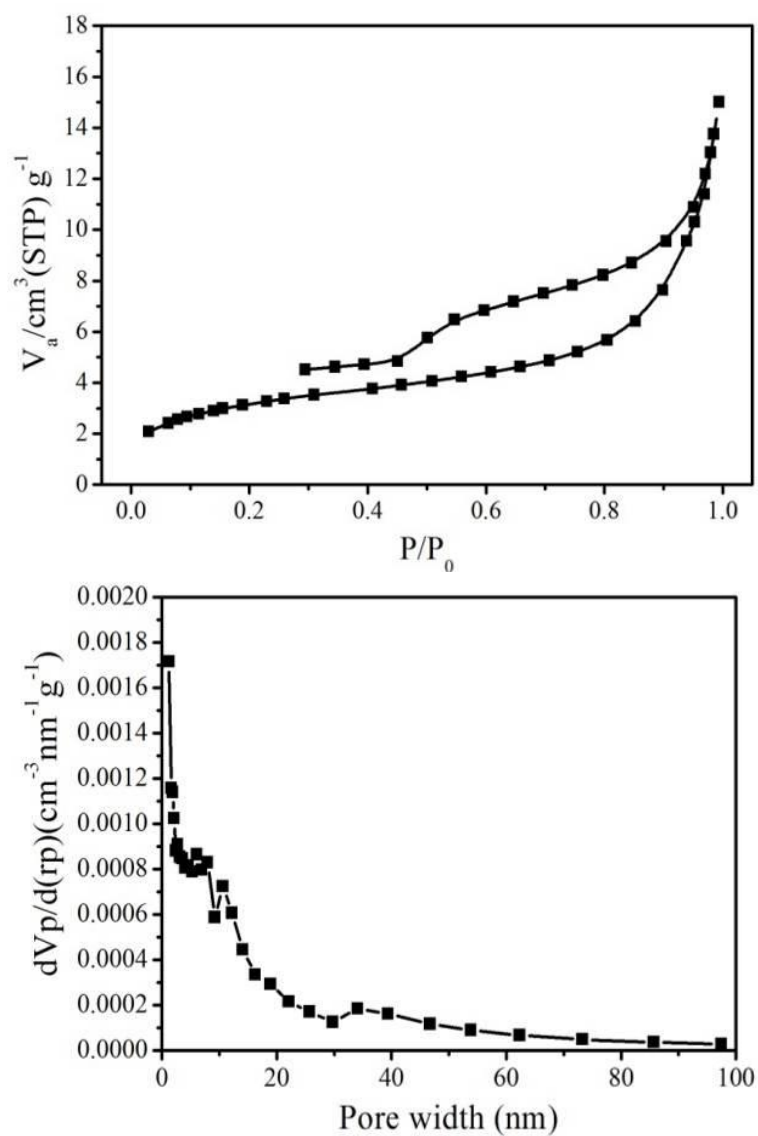


**Figure S4.**  $\text{N}_2$  sorption isotherm (top) and pore-size distribution (bottom) of hierarchically porous ZIF-8/PS after removing the ZIF-8 by acetic acid dissolution.

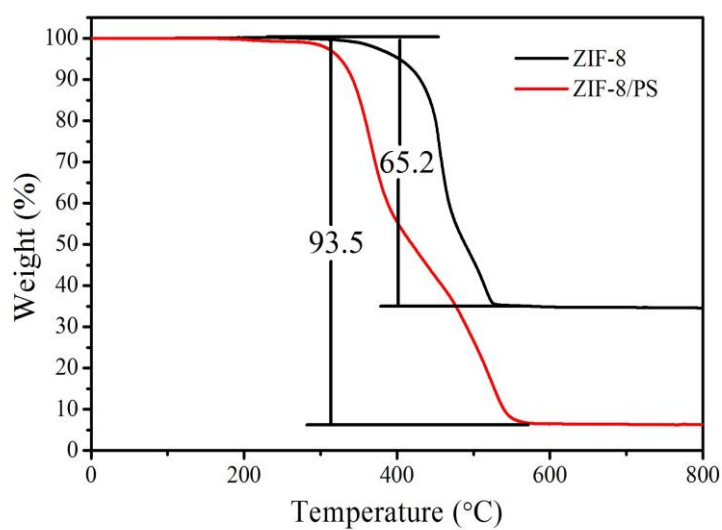


**Figure S5.** TGA data of ZIF-8 nanoparticles and hierarchically porous ZIF-8/PS composites.

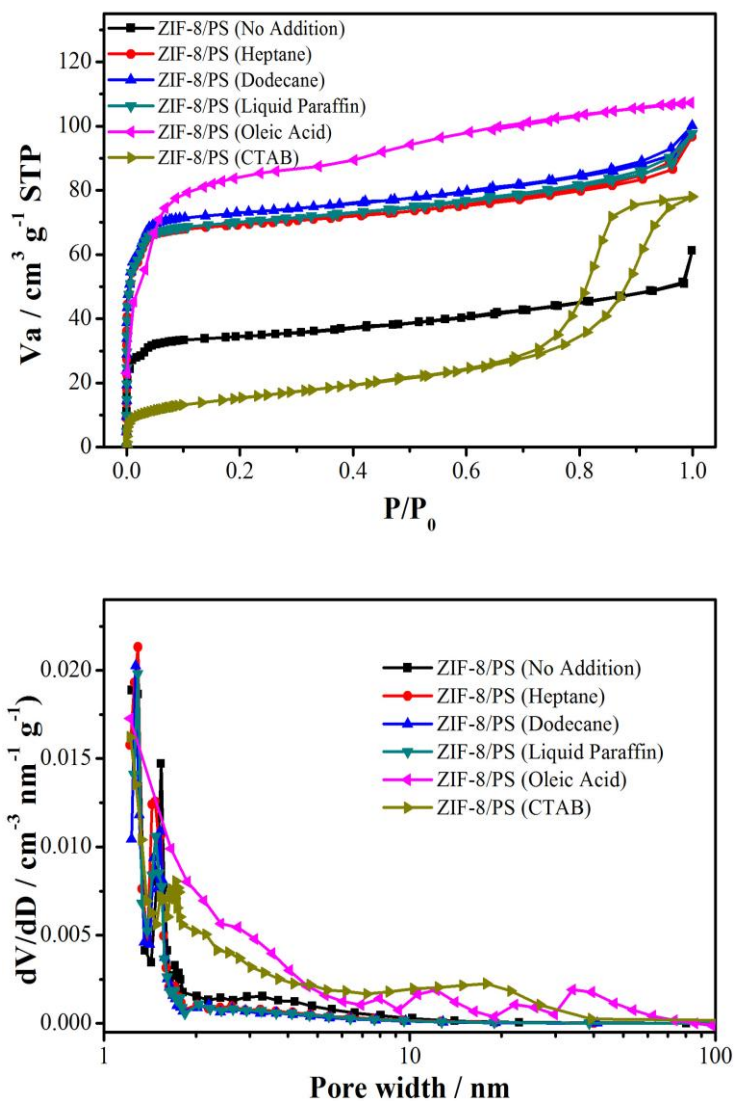
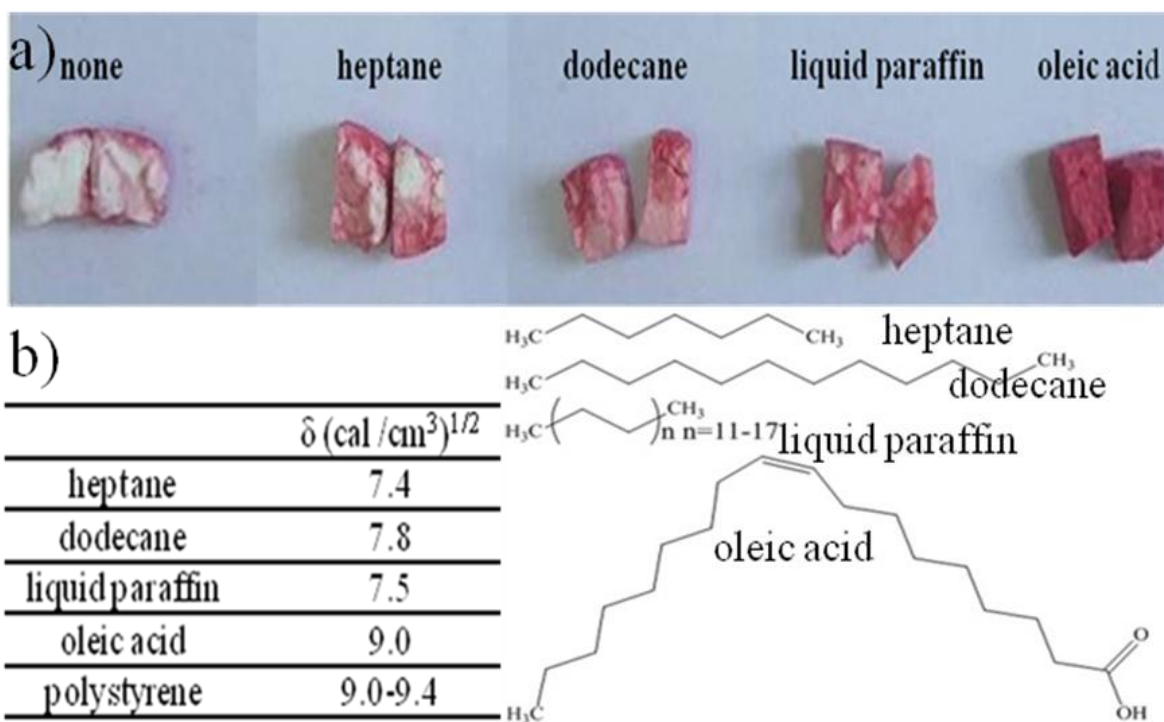


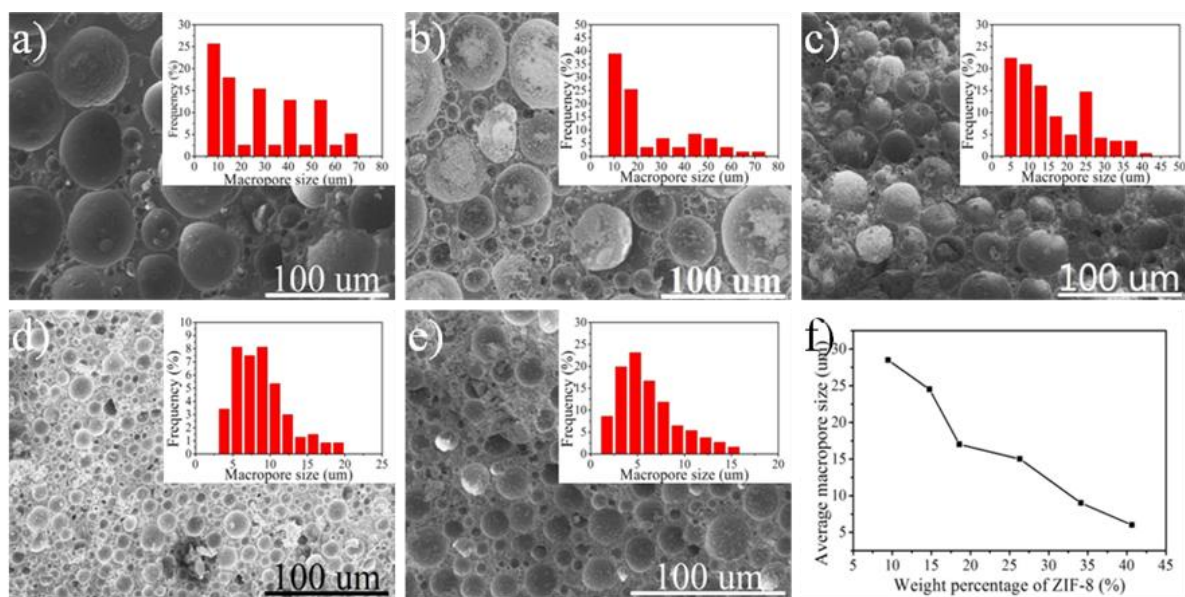
Figure S6. N<sub>2</sub> sorption isotherm (top) and pore-size distribution (bottom) of hierarchically porous ZIF-8/PS prepared without or with different swelling agents .

Table S1. Specific surface area (BET method) of hierarchically porous ZIF-8/PS prepared without or with different swelling agents.

swelling agents	no addition	heptane	dodecane	liquid paraffin	oleic acid	CTAB
BET surface area	133	275	276	279	299	178



**Figure S7.** (a) Photos of split pieces of ZIF-8/PS composites prepared in the presence of different swelling agents after soaking in an ethanolic solution of oil red; (b) The solubility parameters and molecular structures of the swelling agents used.



**Figure S8.** SEM images of the cross-section of ZIF-8/PS composites prepared with different amounts of ZIF-8 nanoparticles: (a) 0.3 g, (b) 0.5 g, (c) 1.2 g, (d) 1.8 g, and (e) 3.0 g (insets show their corresponding macropore size distributions); and (f) the relationship between weight percentage of ZIF-8 added and the average macropore size in the ZIF-8/PS composites.

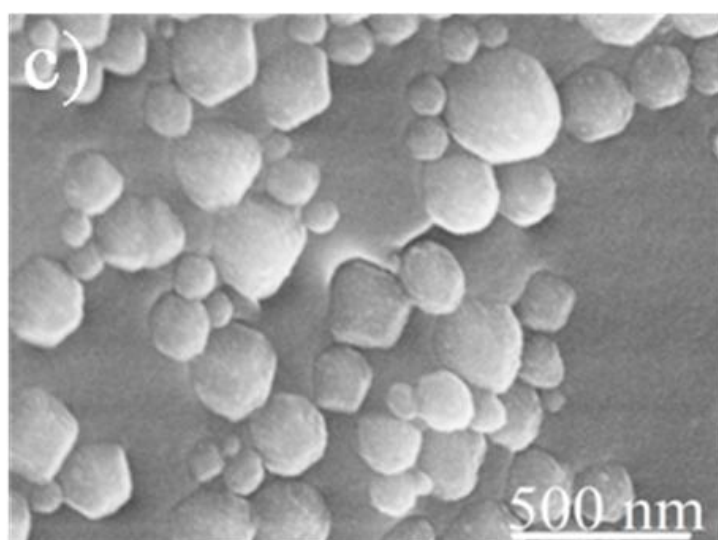
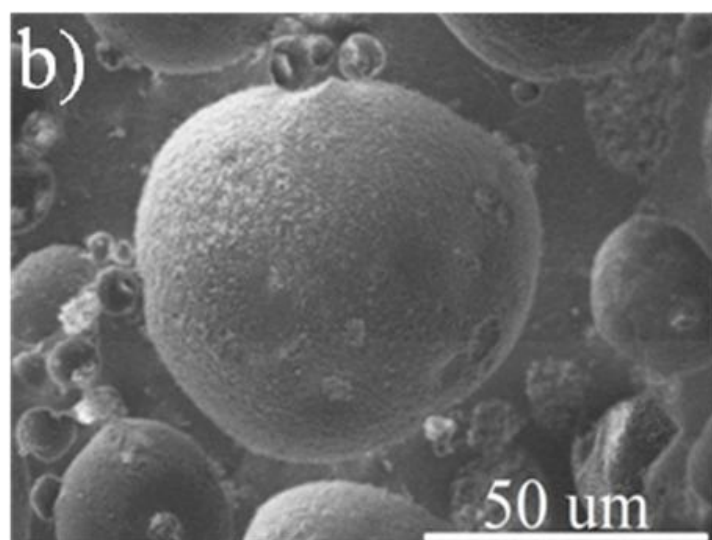
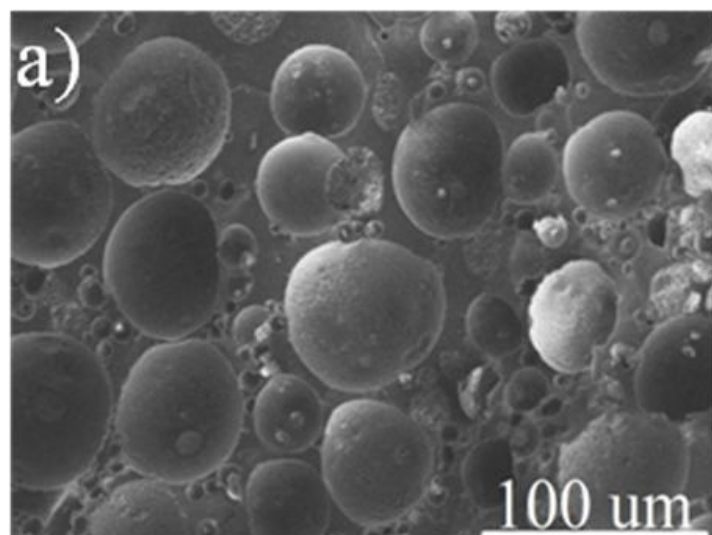


**Figure S9.** Low and high magnification SEM images of the cross-section of hierarchically porous ZIF-8/PS prepared with 0.3 g ZIF-8 nanoparticles.

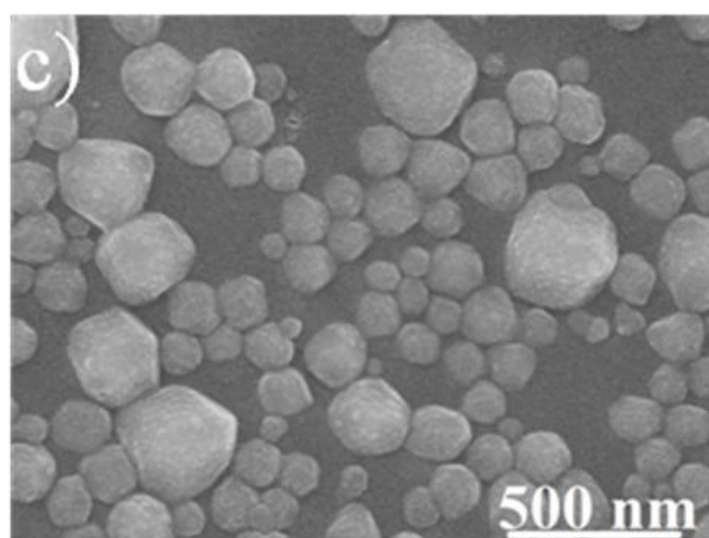
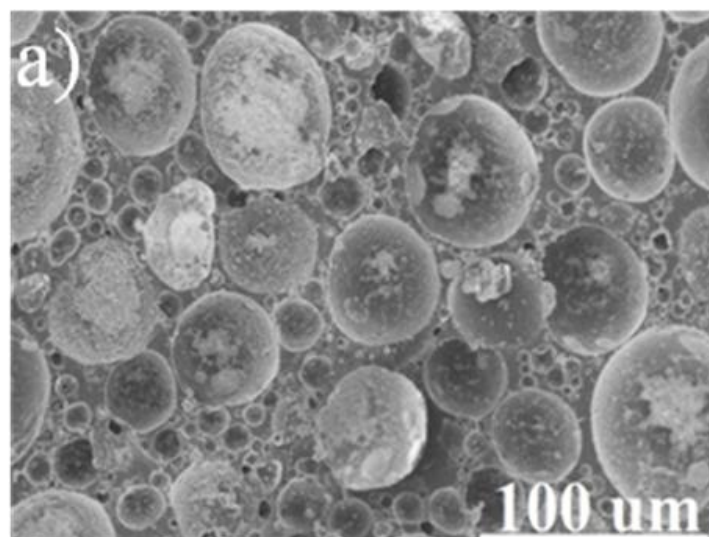


**Figure S10.** Low and high magnification SEM images of the cross-section of hierarchically porous ZIF-8/PS prepared with 0.5 g ZIF-8 nanoparticles.

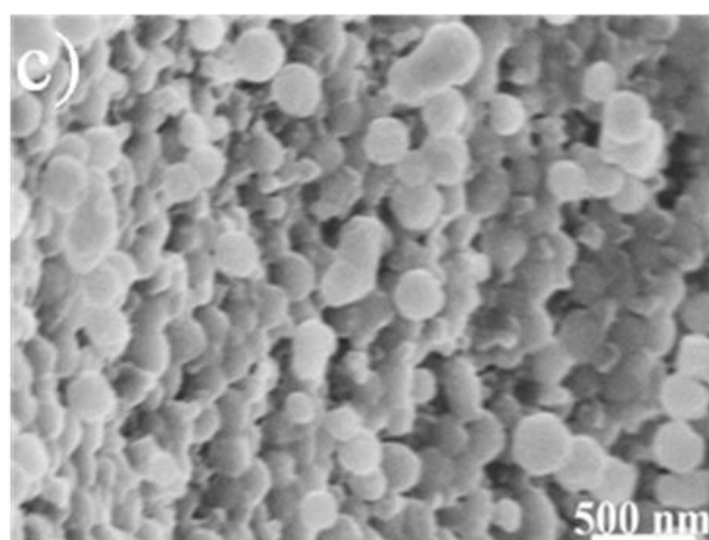
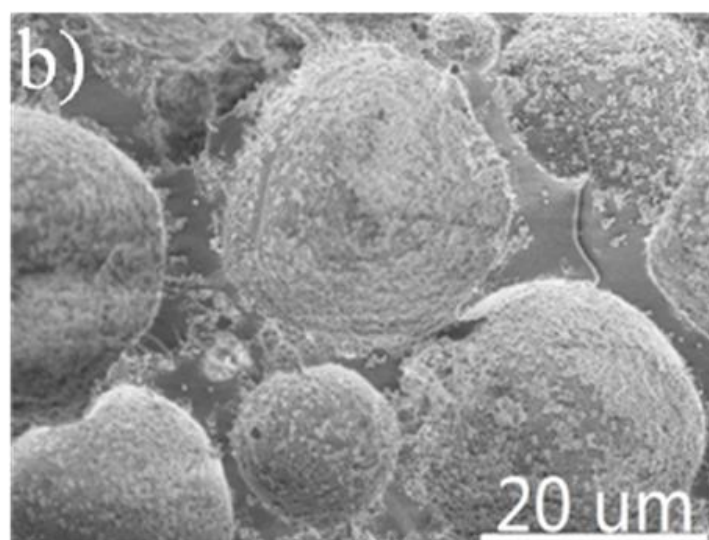
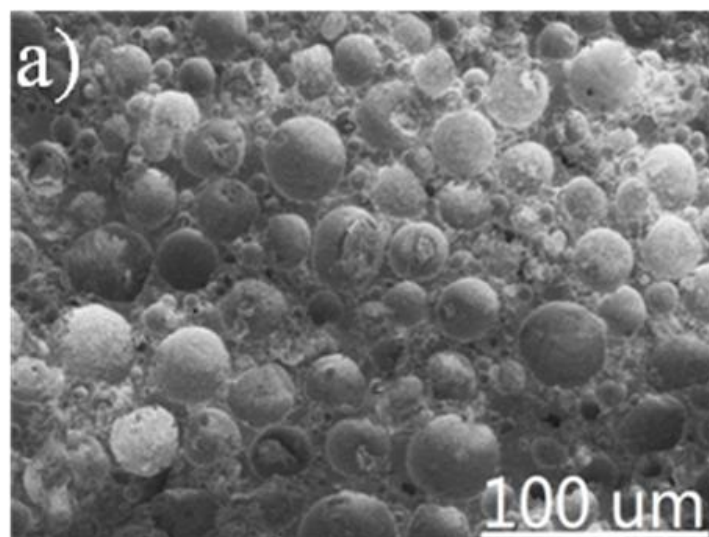


**Figure S11.** Low and high magnification SEM images of the cross-section of hierarchically porous ZIF-8/PS prepared with 1.2 g ZIF-8 nanoparticles.

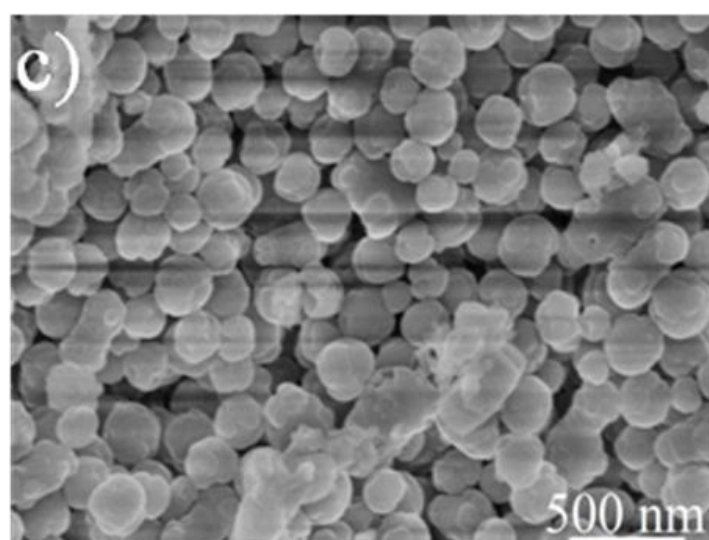
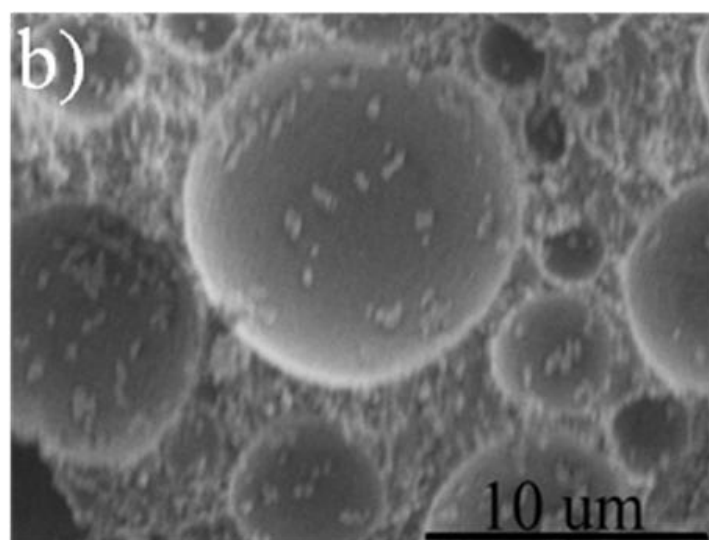
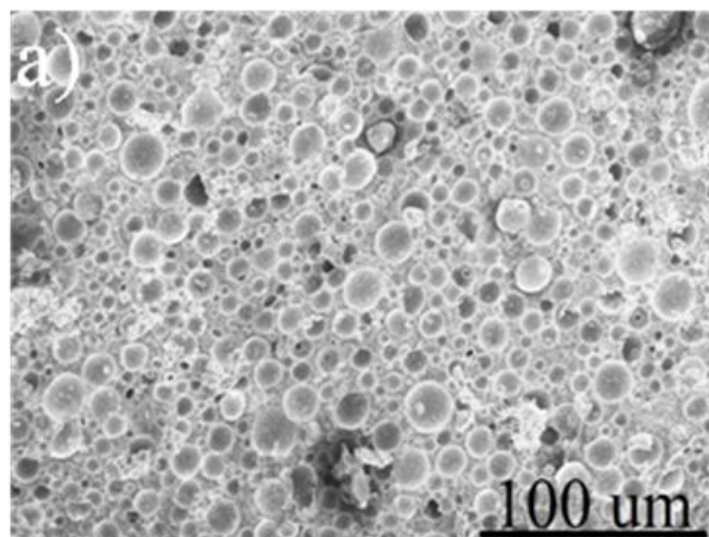


**Figure S12.** Low and high magnification SEM images of the cross-section of hierarchically porous ZIF-8/PS prepared with 1.8 g ZIF-8 nanoparticles.

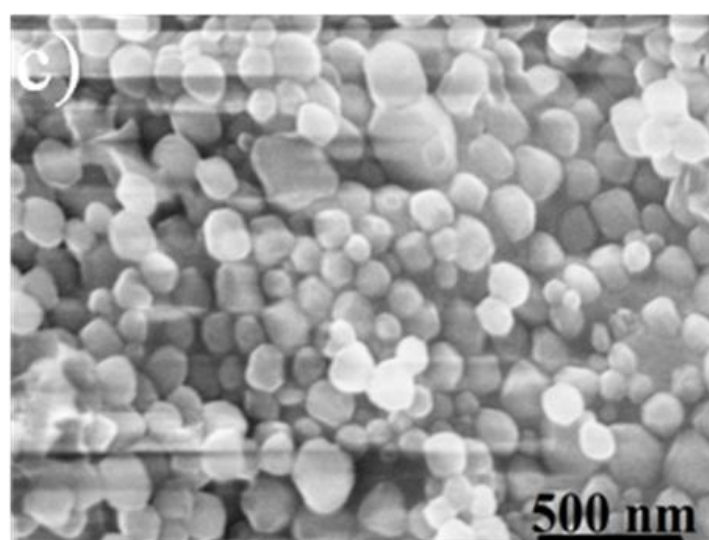
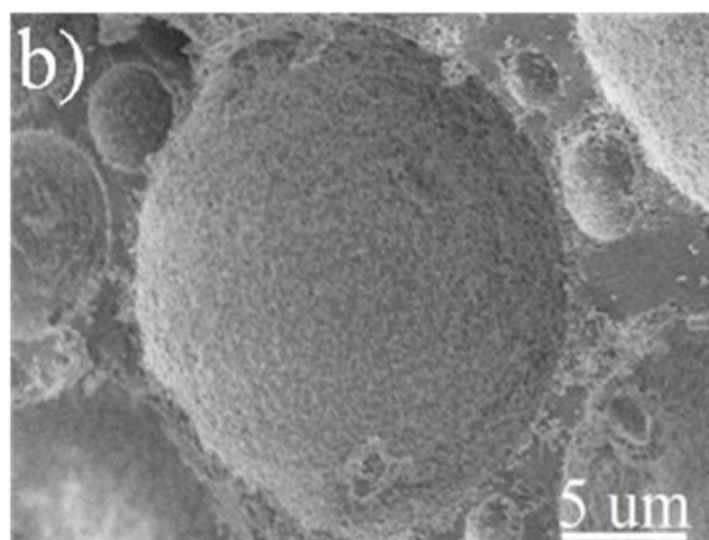
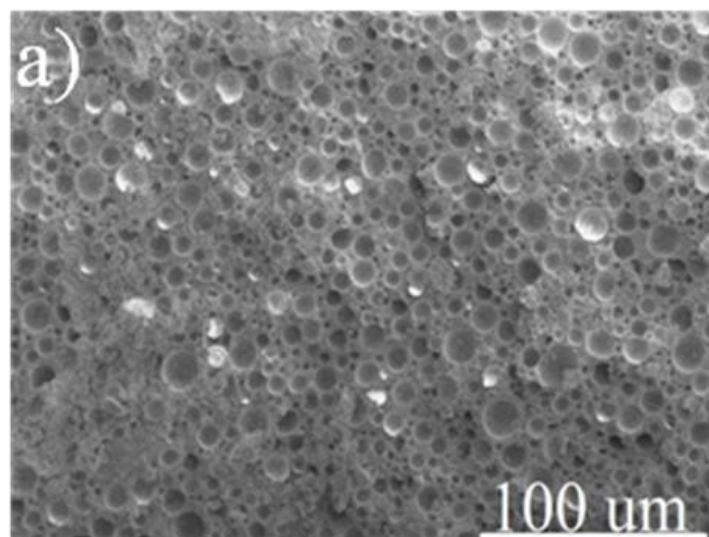


**Figure S13.** Low and high magnification SEM images of the cross-section of hierarchically porous ZIF-8/PS prepared with 3.0 g ZIF-8 nanoparticles.

**Table S2.** Average macropore size of ZIF-8/PS with increasing amounts of added ZIF-8 nanoparticles

ZIF-8	0.3 g	0.5 g	0.7 g	1.2 g	1.8 g	3.0 g
average macropore size (um)	28.5	24.5	17.0	15.0	9.0	6.0

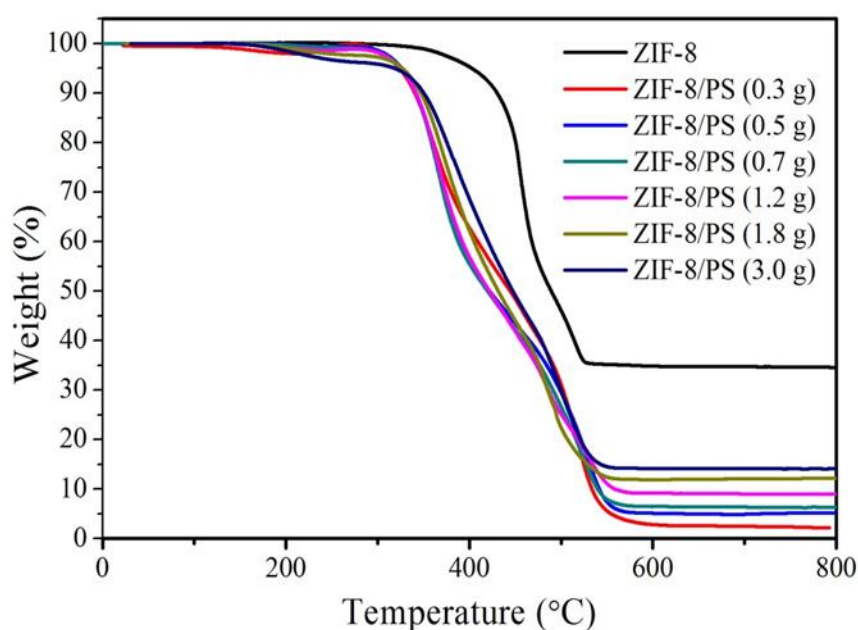


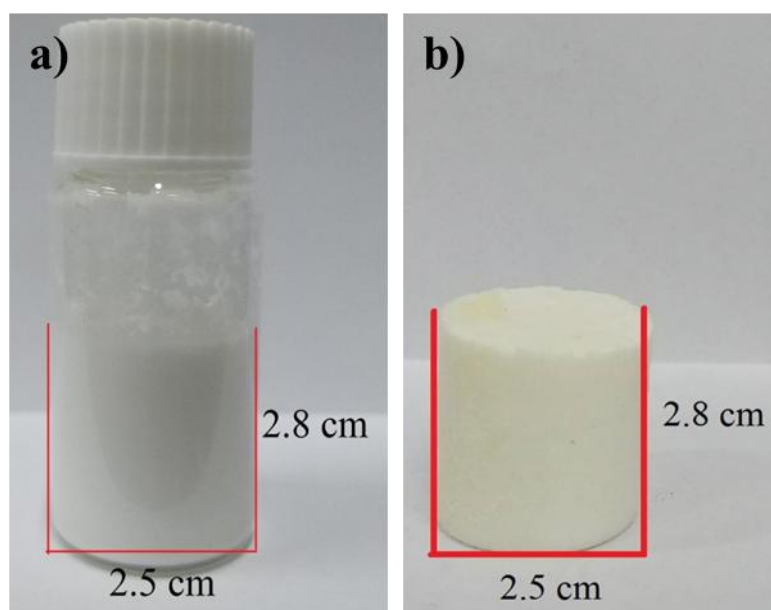
**Figure S14.** TGA data of ZIF-8 and hierarchically porous ZIF-8/PS prepared with different amounts of added ZIF-8 nanoparticles.

**Table S3.** Weight percentage of ZIF-8 within the ZIF-8/PS calculated from TGA data.

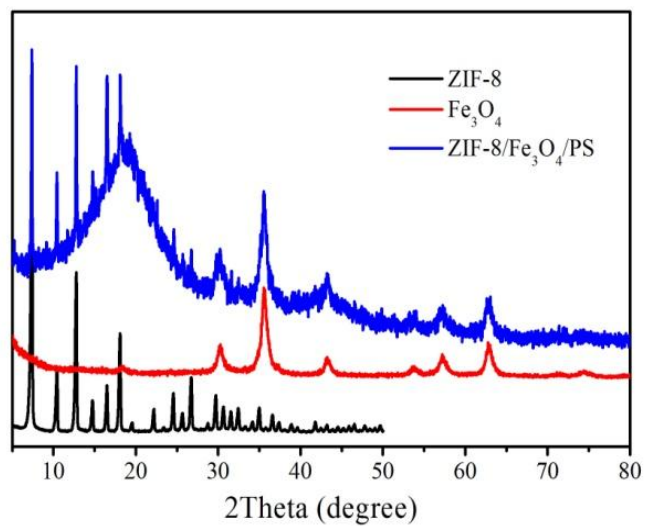
ZIF-8	0.3 g	0.5 g	0.7 g	1.2 g	1.8 g	3.0 g
Weight percentage ZIF-8 (wt%)	7.2	14.8	18.6	26.3	34.1	40.7

Table S4. The comparison of weight percentage of ZIF-8 within the ZIF-8/PS and HKUST-1 within the HUST-1/PAM calculated from TGA or ICP-OES data.

	TGA data	ICP-OES data
Weight percentage ZIF-8 (wt%) within the ZIF-8/PS	18.6	19.1
Weight percentage HKUST-1 (wt%) within the HKUST-1	12.3	11.8



**Figure S15.** Photos of ZIF-8 containing emulsions before (a) and after (b) polymerization. The size of the monolith after polymerization is almost equal to the size of the emulsion in the sample vial before polymerization, indicating the robustness of the monolith and absence of shrinking upon drying.



**Figure S16.** PXRD patterns of ZIF-8 nanoparticles, Fe<sub>3</sub>O<sub>4</sub> nanoparticles and hierarchically porous ZIF-8/ Fe<sub>3</sub>O<sub>4</sub>/PS ternary composites demonstrating the successful incorporation of both the framework and the magnetite.

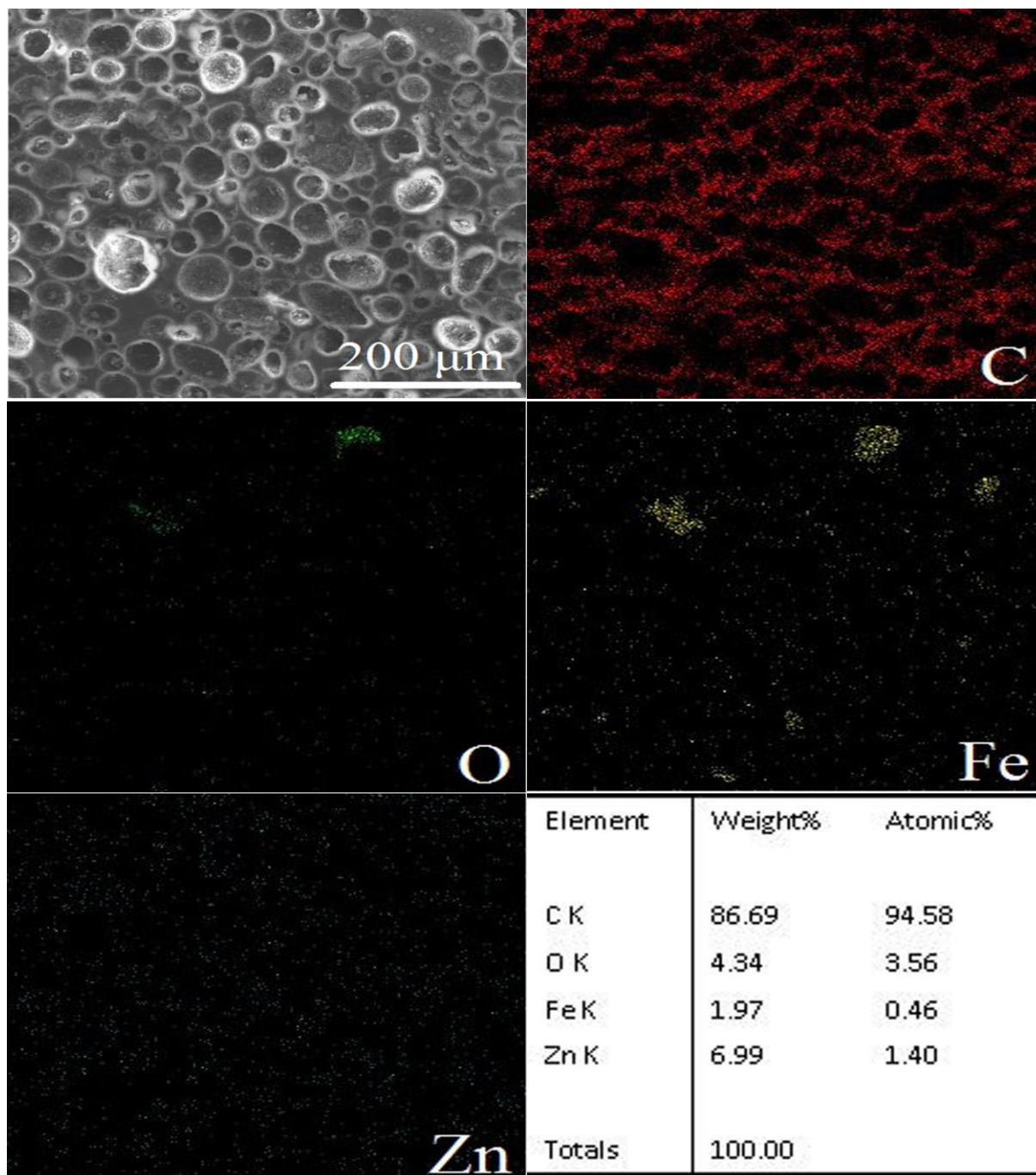
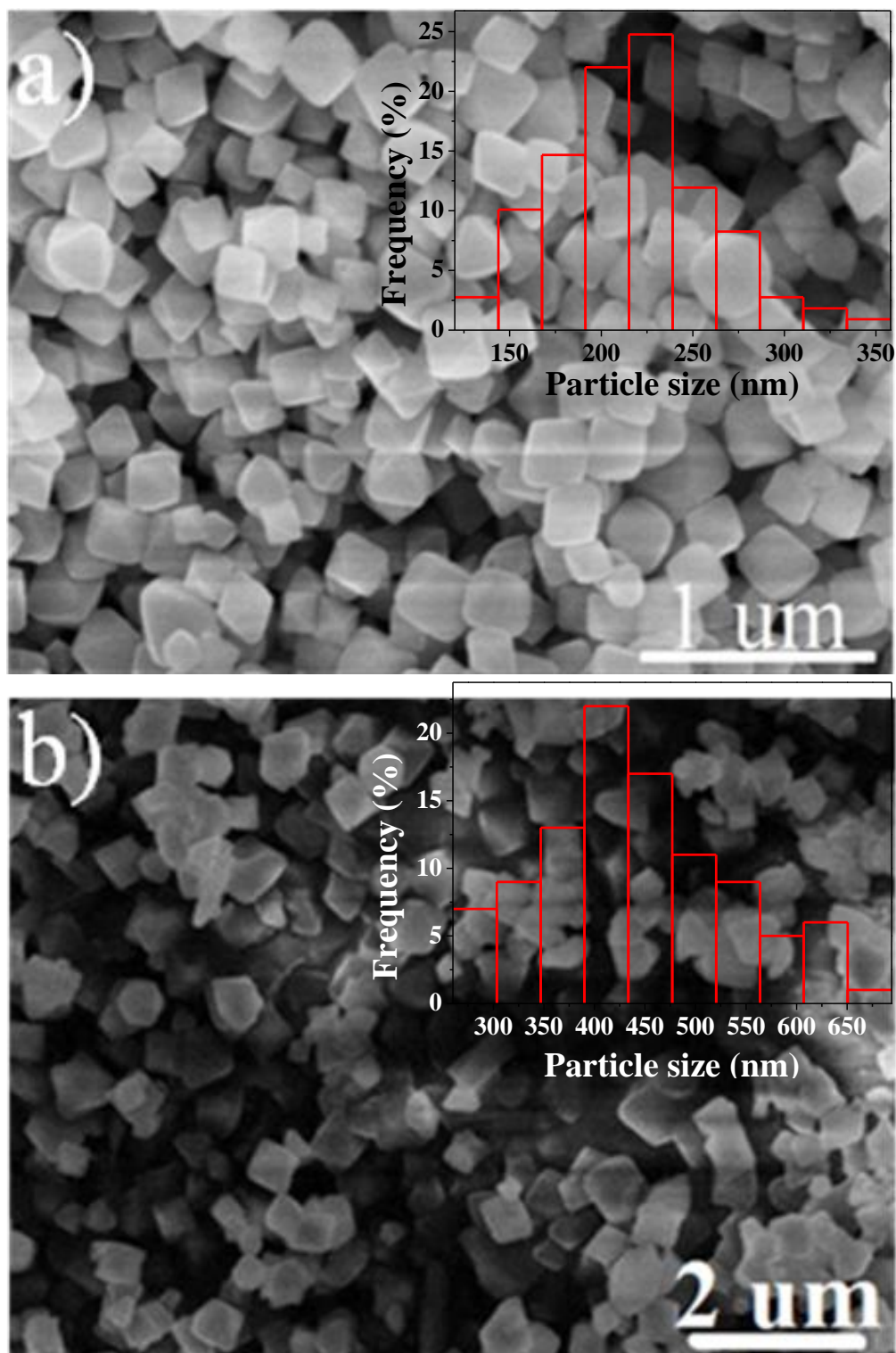


Figure S17. EDS-Mapping of hierarchically porous ZIF-8/  $\text{Fe}_3\text{O}_4$ /PS.

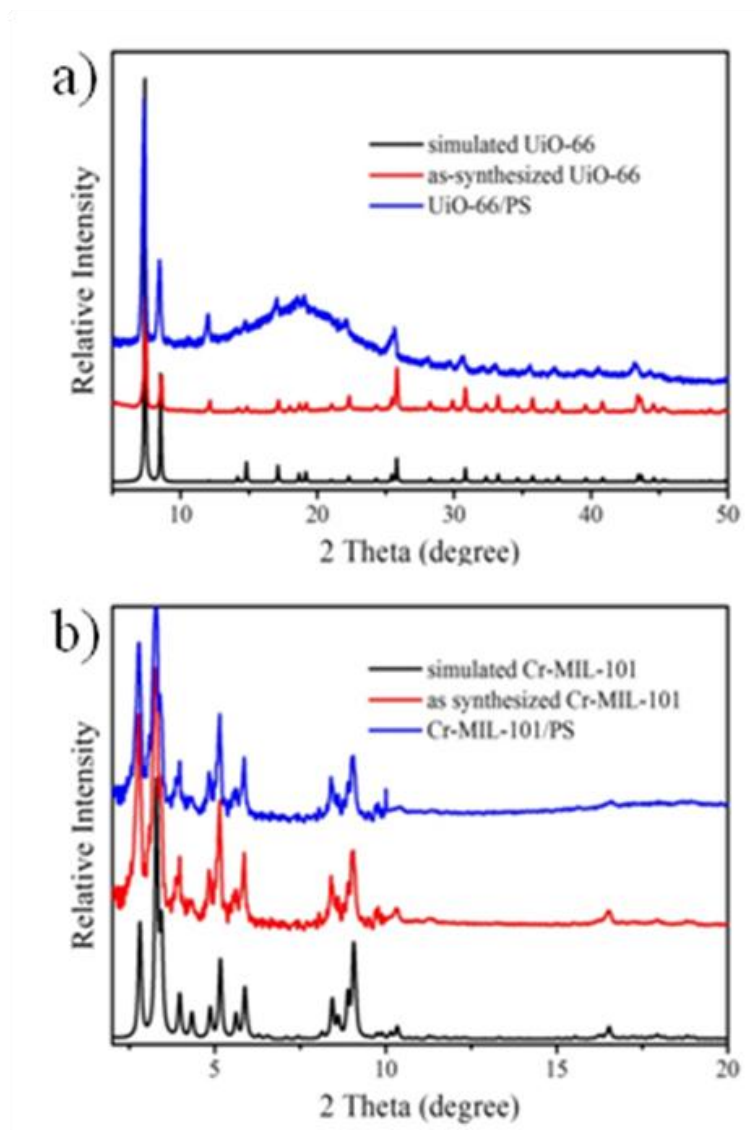


Figure S 18. Photos of the ZIF-8/PS before being stirred in the toluene (left) or water (right).

### S3. Generality of interfacial nanoassembly/ emulsion polymerization



**Figure S19.** SEM images of the as-synthesized UiO-66 nanoparticles (average size is 216 nm) (a) and Cr-MIL-101 nanoparticles (average size is 442 nm) (b) used to stabilise Pickering emulsions prior to polymerisation of the continuous phase (Insets are their corresponding particle size distribution).



**Figure S20.** PXRD patterns of UiO-66 nanoparticles and hierarchically porous UiO-66/PS (a) and those of Cr-MIL-101 nanoparticles and hierarchically porous Cr-MIL-101/PS (b).

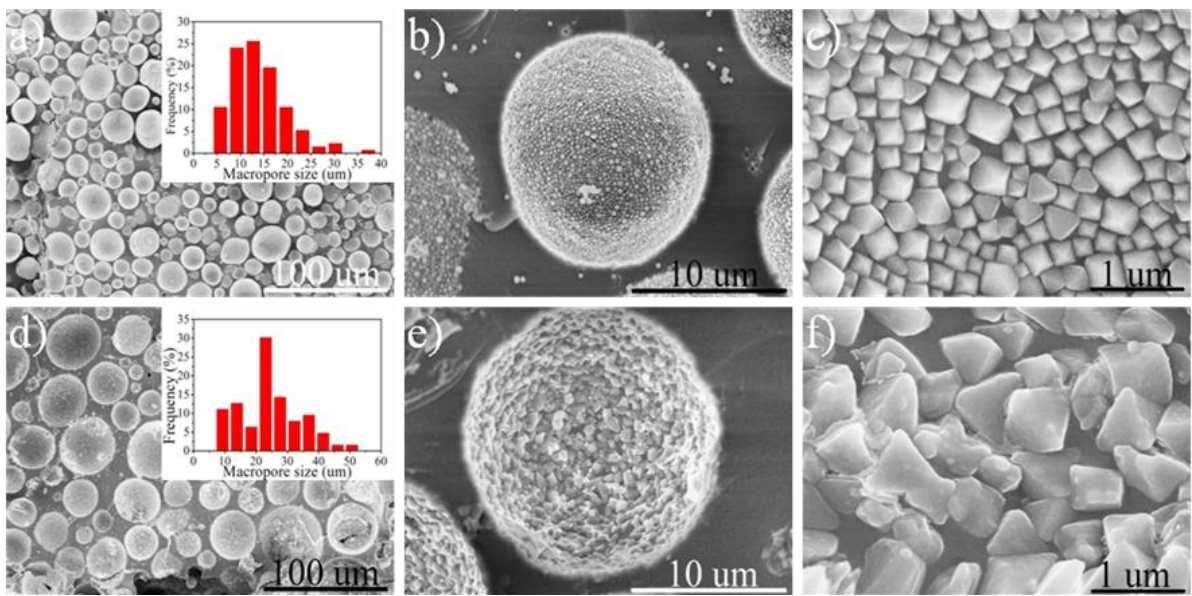


**Figure S21.** Low and high magnification SEM images of the cross-section of hierarchically porous UiO-66/PS (a-c) and Cr-MIL-101/PS (d-f) composites. The insets in (a) and (d) show the corresponding macropore size distributions.

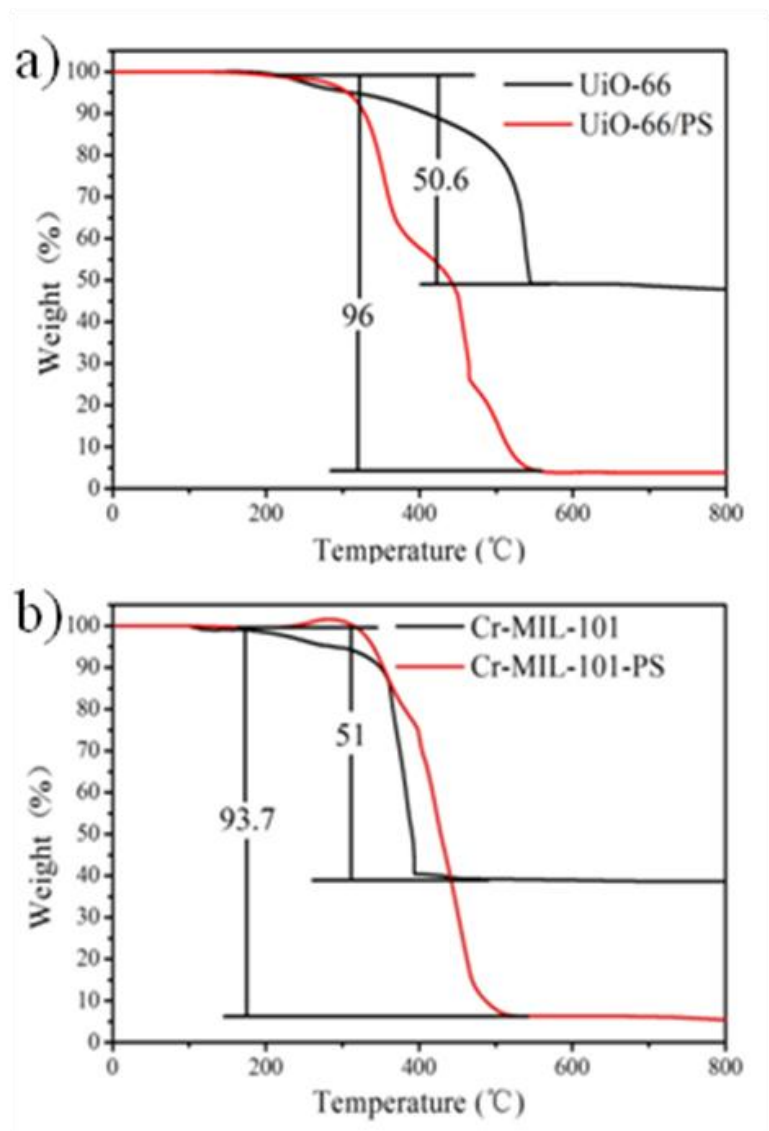


**Figure S22.** TGA data of UiO-66 nanoparticles and hierarchically porous UiO-66/PS (a) and those of and Cr-MIL-101 nanoparticles and hierarchically porous Cr-MIL-101/PS (b).

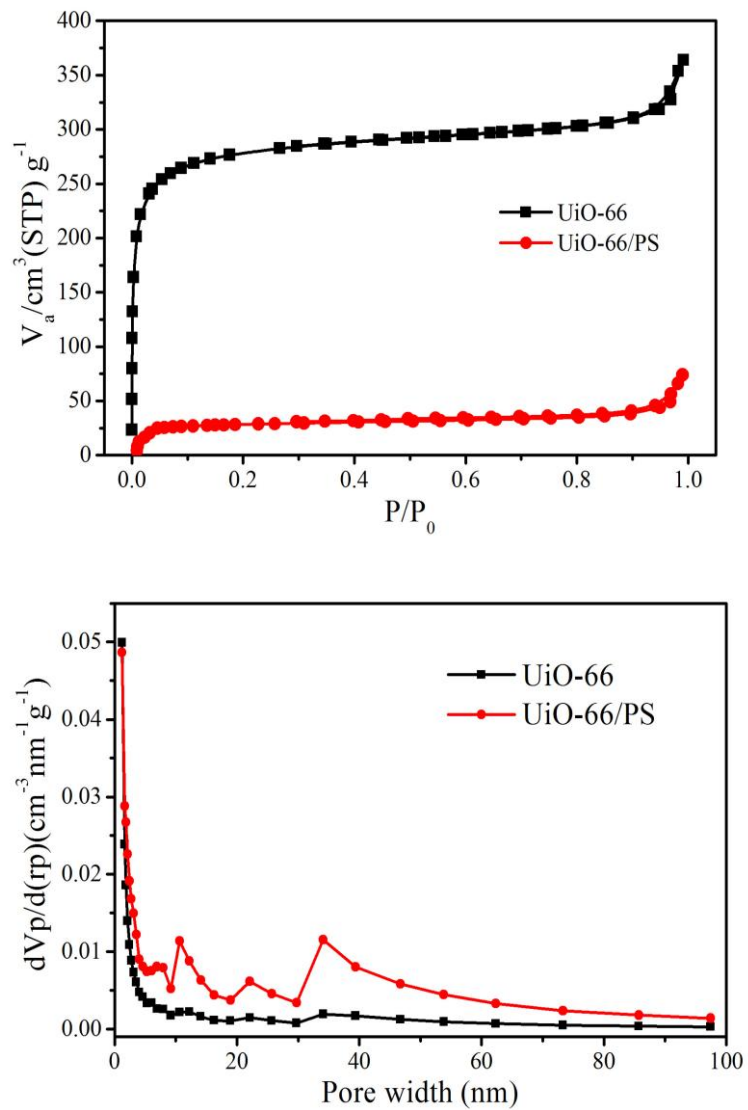


**Figure S23.**  $\text{N}_2$  sorption isotherm (top) and BJH pore-size distribution (bottom) of UiO-66 and hierarchically porous UiO-66/PS.

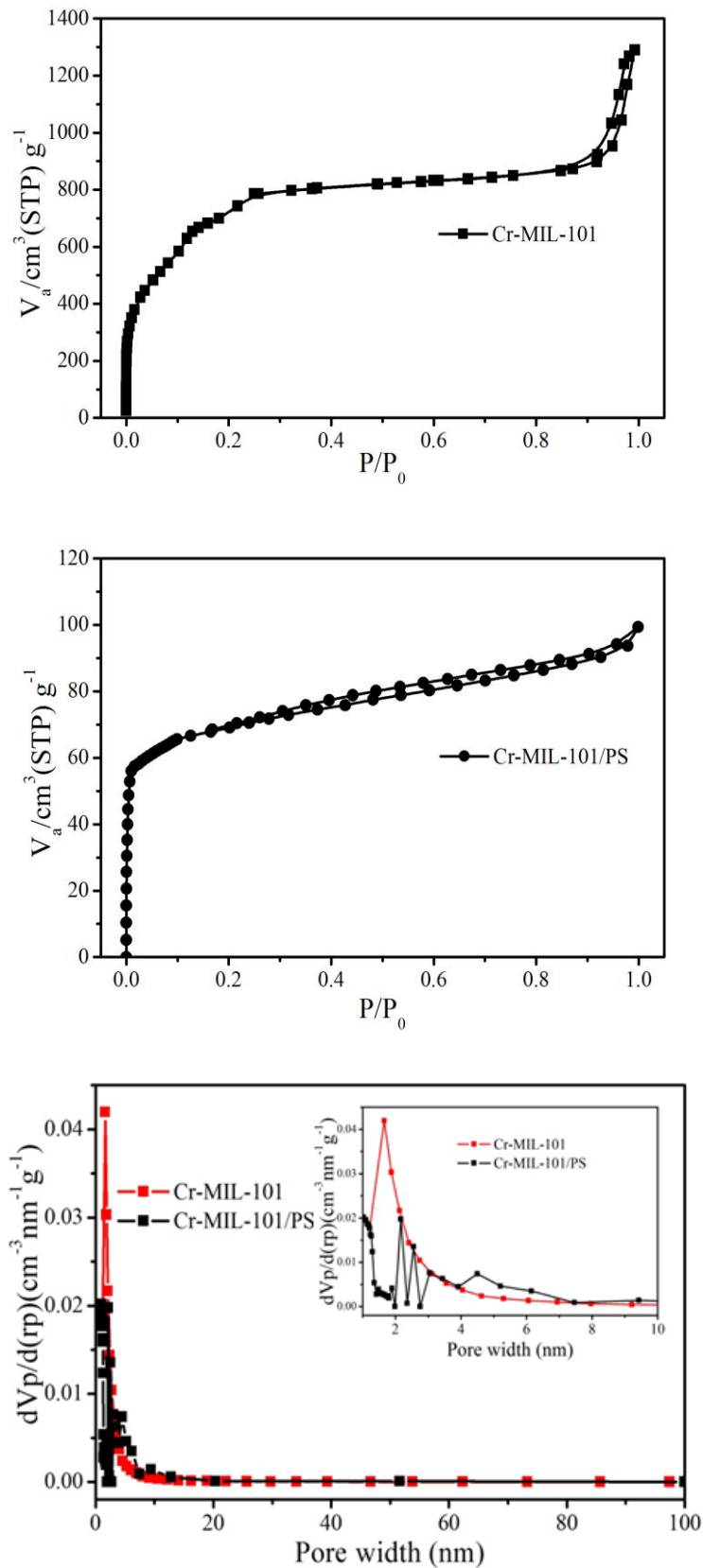


**Figure S24.**  $\text{N}_2$  sorption isotherms of Cr-MIL-101 (top) and hierarchically porous Cr-MIL-101/PS (middle); and BJH pore-size distribution of Cr-MIL-101 and hierarchically porous Cr-MIL-101/PS (bottom).

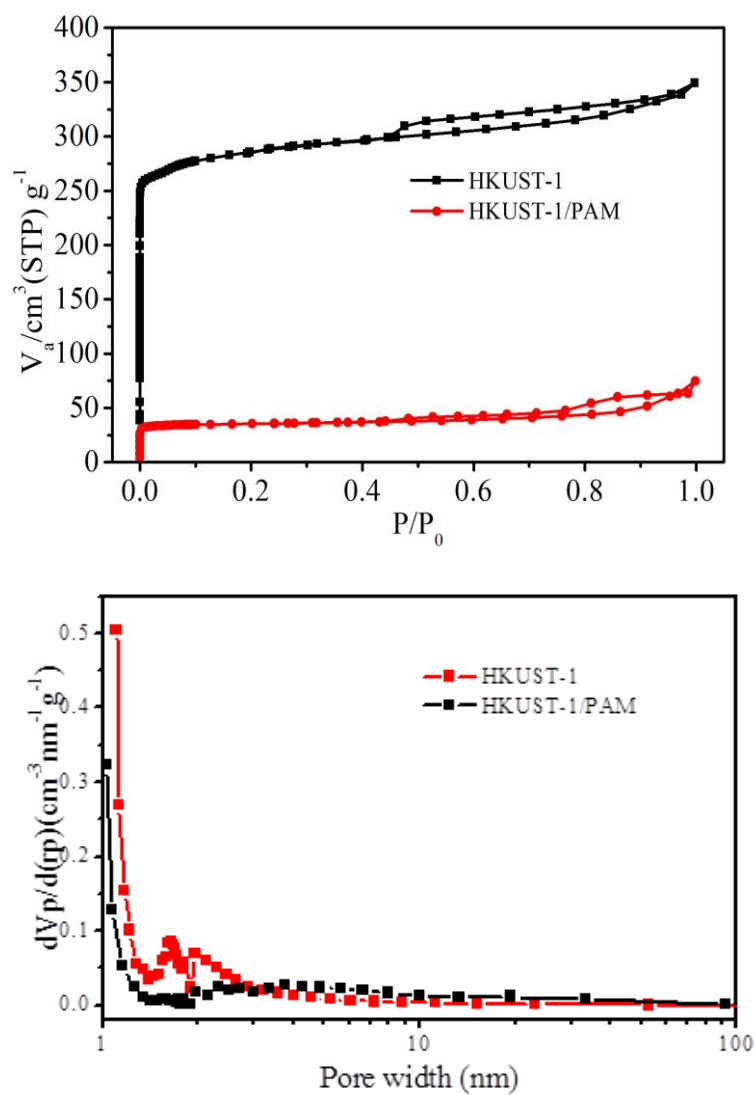


**Figure S25.**  $\text{N}_2$  adsorption isotherm (top) and BJH pore-size distribution (bottom) of HKUST-1 and hierarchically porous HKUST-1/PAM.

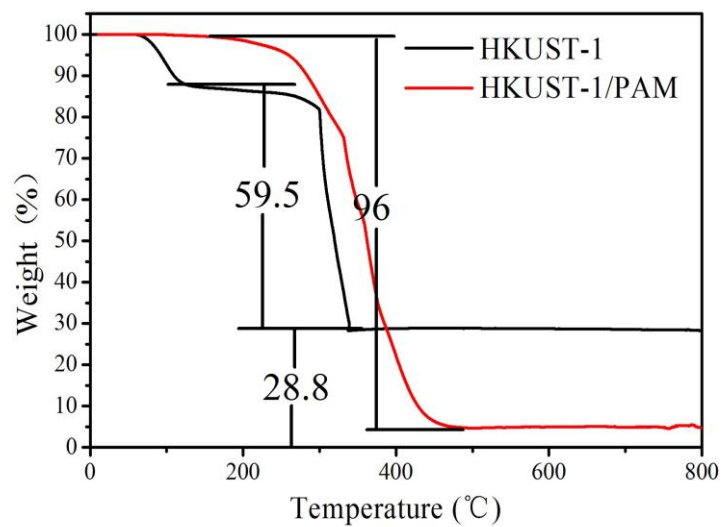


**Figure S26.** TGA data of HKUST-1 nanoparticles and hierarchically porous HKUST-1/PAM.

#### S4. Knoevenagel condensation reaction catalyzed by ZIF-8-based catalysts

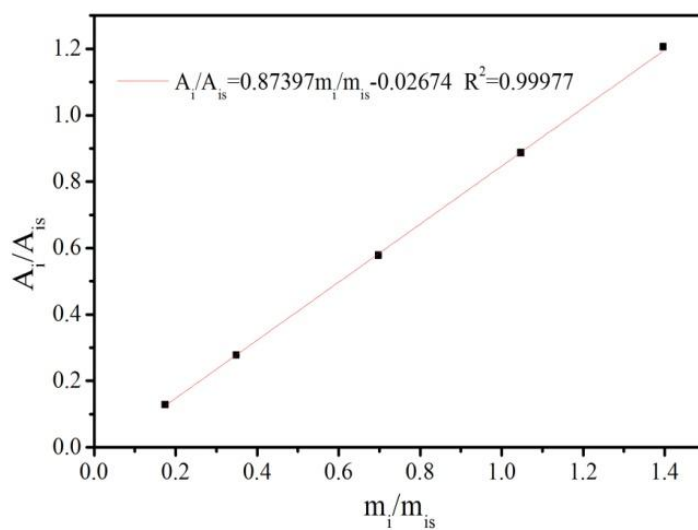


**Figure S27.** The standard absorption curve of benzaldehyde with dodecane as the internal standard.

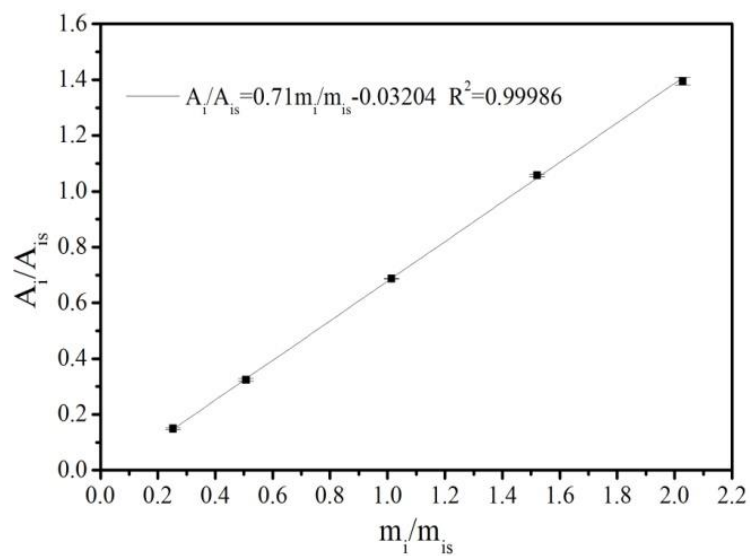


**Figure S28.** The standard absorption curve of benzylidenemalononitrile with dodecane as the internal standard.

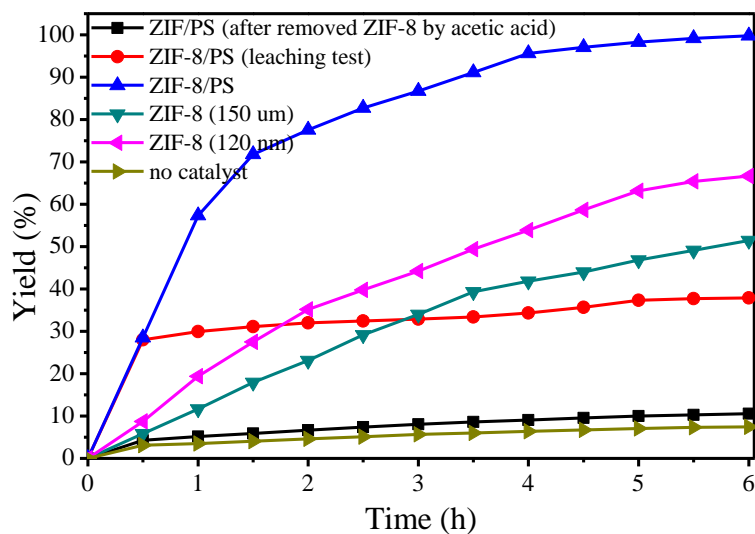


**Figure S29.** The relationship between the yield of benzylidene malononitrile and reaction time of the Knoevenagel condensation reaction catalyzed by ZIF-8/PS based catalysts. (The yield of benzylidene malononitrile was calculated from the amount of the product to demonstrate the benzaldehyde was completely converted into benzylidene malononitrile).

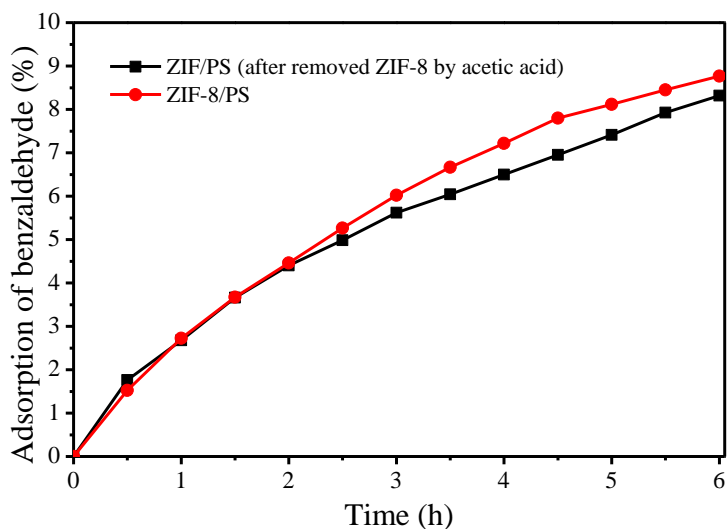


**Figure S30.** Benzaldehyde adsorption curves from toluene solution (0.36 mol/L) of ZIF-8/PS before and after removal of ZIF-8 with acetic acid.

1. J. Huo, M. Marcello, A. Garai and D. Bradshaw, *Adv. Mater.*, 2013, **25**, 2717-2722.
2. L. H. Wee, M. R. Lohe, N. Janssens, S. Kaskel and J. A. Martens, *J. Mater. Chem.*, 2012, **22**, 13742-13746.